Hindawi
Advances in Materials Science and Engineering
Volume 2017, Article ID 2493921, 13 pages
https://doi.org/10.1155/2017/2493921

Research Article

Study on Fracture Initiation and Propagation in a Brazilian Disc with a Preexisting Crack by Digital Image Correlation Method

Lin Luo, Xibing Li, Jiadong Qiu, and Quanqi Zhu

School of Resources and Safety Engineering, Central South University, Changsha 410083, China

Correspondence should be addressed to Lin Luo; csulinluo1991@csu.edu.cn

Received 10 January 2017; Revised 14 April 2017; Accepted 23 April 2017; Published 24 May 2017

Academic Editor: Hiroshi Noguchi

The effect of a preexisting crack with different inclination angles and lengths on mechanical properties, fracture initiation, and propagation in a Brazilian disc was investigated in this paper. In the experiment, digital image correlation (DIC) method was employed to record the deformation in the specimen. Different failure patterns, depending on inclination angles and lengths of the preexisting crack, were observed. The fracture initiation position deviates from the tips of the preexisting crack with the inclination angle increasing from 0° to 72° at an interval of 18° per increment. Secondary cracks are more likely to occur in the Brazilian disc with a more inclined and longer preexisting crack. A finite-discrete element combined method ELFEN was used in the numerical investigation to simulate the failure process. This investigation shows that there are good correlations between the experimental and numerical results. Digital image correlation is a good method to obtain the quantitive full-field strain distribution and to observe the strain evolution process in a jointed rock.

1. Introduction

As the main material of mining and civil engineering, rock deformation and failure may cause interruption in mining and building activities, or even significant safety hazards [1–3]. With the growing demands for resources and the substantial increase in underground activities, rock mechanical behavior is of major importance in civil projects, mining engineering, and mineral exploration related operations [4]. Rock mass usually contains a large number of microcracks, voids, and microdefects due to environmental effects during the diagenetic process. This emphasizes the need to better understand the failure of rock structures consisting of flaws and cracks.

To study the tensile characteristics of rock-like materials, the Brazilian test is an indirect method that has been suggested by the International Society for Rock Mechanics [5] because of convenient specimen preparation and simple test implementation. Zhou et al. [6] extended the Brazilian disc test to the coupled static and dynamic load condition. Dynamic Brazilian tests were conducted on layered phyllite specimens by Qiu et al. [7] to investigate the dynamic mechanical response of layered rocks. Luo et al. [8] studied static and dynamic tensile behaviors of rock-shotcrete interface under the Brazilian test. A Brazilian disc with a preexisting inclined crack is a classic case of mixed mode fracturing. Early work was done by Awaji and Sato [9] and Atkinson et al. [10] in the 1970s and 1980s, who gave explicit results of stress intensity factors (N_I and N_{II}) depending on the notch length and inclination angle and then determined the Mode I and Mode II fracture toughness by using this centrally cracked disc. Jia et al. [11] firstly employed laser holographic interferometry and reflection photoelasticity to study the fracture properties of center notched concrete specimens subjected to combined stress condition with the effect of the loading rate. In recent years, a Brazilian test with a preexisting inclined crack has been a subject of considerable research interest. Geometry and size effect on the fracture trajectory in a limestone rock under mixed mode loading was investigated experimentally and theoretically by Aliha et al. [12] and it was then stated that the size affects the initiation angle, while it has no significant effect on the fracture trajectory. Erarslan and Williams [1] conducted static and cycling diametrical compression tests on the inclined cracked chevron notched Brazilian disc and found that the opening or closure of the preexisting crack, the crack initiation angle,

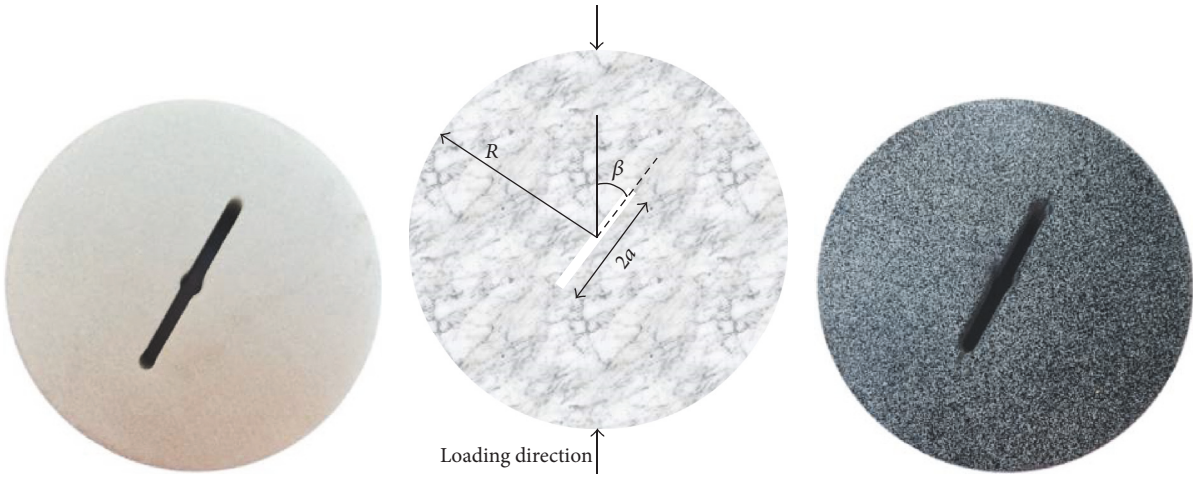

Figure 1: Pictures of the central straight through Brazilian discs (CSTBD): (a) a central notched Brazilian disc; (b) the geometry of the CSTBD; (c) a typical speckle pattern.

and initiation point are strongly influenced by its inclination angle and the loading condition. Fracture initiation and propagation, depending on the frictional resistance of the preexisting crack, were studied by Cai [13] using a finite-discrete element combined method ELFEN. It was observed that the wing crack's initiation locations deviate from the crack tips and the secondary cracks also deviate slightly from the in-line direction of the preexisting crack as the frictional resistance increases. A full-field stress distribution at two stages was also presented in his investigation as many scholars did. However, few studies have focused on the global strain field in the disc specimen with a preexisting crack.

The measurement of rock deformation is of great importance for the experimental study on rock mechanics and the method we often used is strain gauge method. However, the inhomogeneous deformation generated in the precracked disc cannot be simply reflected by strain gauges because strain gauges can only be used for a single point, and they are incapable of revealing a global strain response to the applied loads. In recent years, therefore, some optical methods such as Moiré interferometry [14], holographic method [15], photoelastic method [15, 16], and digital image correlation method [17] have been developed and employed in some fracture tests. Based on the advantages such as full-field noncontact, low environmental requirements, and excellent adaptability, DIC method, short for digital image correlation method, has drawn rather considerable interest in the past decades. Ma et al. [17] designed a Geo-DSCM system to analyze the damage evolution and failure procedure of a borehole rock structure and reported that the deformation localization initializes at the vulnerable area of the structure. Experimental investigation on the failure process of brittle materials with a preexisting open-hole defect was carried out by utilizing a 3D digital image correlation method [18]. Three-dimensional digital image correlation was also applied in uniaxial compression tests on sandstone by Munoz et al. [19] and the prepeak coupled with postpeak strain characteristic during the compression was provided by this 3D DIC method in a straightforward way. Lin et al. [20, 21] performed fracture tests on sandstone specimens under three-point bending, in which the maximum crack opening displacement and the length of the localized damage zone were measured by the digital image correlation method. A series of experiments based on DIC technique have been conducted by Ji et al. [22, 23] and a detailed analysis was performed to determine the fracture modes. All these studies indicate that DIC method shows its superiority in crack initiation, propagation, and failure process in experimental studies on rock mechanics.

In this paper, fracture initiation and propagation in a Brazilian disc with a preexisting crack have been studied experimentally with the aid of DIC method and numerically using a finite-discrete element combined method ELFEN, with particular attention to the inclination angle and length of the preexisting crack. The main objectives are (i) to identify how the inclination angle and length will affect fracture initiation, propagation, and failure process and (ii) to investigate the applicability of the DIC method to crack propagation under static diametral compressive loading. The full-field strain distribution in the notched disc was also given dynamically using the DIC method.

2. Specimen Preparation and Testing Procedure

2.1. Specimen Preparation. A metamorphic rock, that is, marble from Hunan, China, was used in the experiment. Marble cores were drilled from a bulky block and were then sliced into discs with an identical thickness (20 mm). Water-jetting equipment with a 0.8 mm diametral nozzle was employed to prepare a straight through notch (see Figure 1(a)) and a diamond wire saw with a piece of 0.26 mm wide wire was used to obtain a sharp crack tip. The geometry of the central straight through Brazilian disc (CSTBD) is illustrated in Figure 1(b). The radius of the specimens, R, is 25 mm,

Table 1: Parameters of the marble material.

Specimen	Density (kg/m^3)	UCS (MPa)	Young's modulus E (GPa)	Poisson's ratio (μ)	σ_t (MPa)
Marble	2780.78	133.97	41.42	0.25	4.97

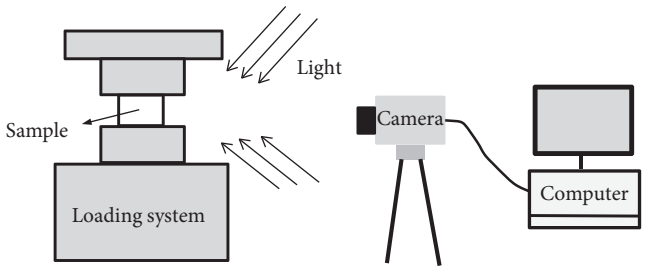

Figure 2: The schematic diagram of the image acquisition system: loading system, light source, a digital camera, and a computer.

and their aspect ratio (i.e., thickness-to-diameter ratio) is maintained at 0.4. The central crack length, $2a$, varies from 15 mm to 20 mm to 25 mm. The inclination angle, β, is defined as the angle between the loading direction and the preexisting crack plane. The end faces and sides of specimens were prepared as smooth and straight to satisfy the recommendations of the International Society for Rock Mechanics [5]. Table 1 lists material parameters of the marble, including the density (ρ), the uniaxial compressive strength (UCS), tensile strength (σ_t), Young's modulus (E), and Poisson's ratio (μ).

The full-field deformation in the notched discs was obtained owing to the application of the DIC method, which relies on a contrasting random texture as a speckle pattern on the surface of the specimen [24]. The artificial speckle pattern was created by the following steps: firstly, white paint was evenly sprayed onto the surface as a base coat; then, black paint was randomly sprayed onto the same surface after the base color was dried [25, 26]. The speckle pattern is required to be nonrepetitive, isotropic, and contrasty enough to permit the software to be able to identify and to calculate the deformations. A typical speckle pattern on the object is shown in Figure 1(c).

2.2. Digital Image Correlation Method. The DIC method is an optical technique which utilizes the full-field, noncontact, and high precision measurement of deformations and displacement. The system consists of an image acquisition system and calculation software named GOM Correlate from a German company.

The image acquisition system, as sketched in Figure 2, includes a monochrome digital camera, a computer, a loading system, and stable light sources [22]. Firstly, adjust the sampling frequency of the digital camera depending on the loading rate; secondly, ensure the stability of light sources to obtain essentially constant grey value; then, acquire digital images of the speckle pattern created on the specimen surface continuously using the monochrome digital camera; finally, store these images into the computer via data transfer services [23].

This calculation technique starts with a reference image taken before loading, which is compared with a series of pictures during the loading period [24, 27]. An assumption is proposed that the grey value of the images remains the same before and after the deformation [23]. First of all, select a region of interest (ROI) on the specimen surface; then, divide this region into numbers of subsets; search for the corresponding subsets after deformation based on the assumption and calculate their displacement; finally, a deformation or displacement distribution map is created thereafter [21, 28].

2.3. Loading Setup and Test Procedure. As shown in Figure 3, rock specimens were subjected to quasi-static load by a servo-controlled hydraulic machine (MTS Landmark system by MTS Inc.), whose stiffness is enough to avoid elastic energy to accumulate in the machine, in the Advanced Research Center at Central South University. This testing machine has a loading capacity of 100 kN and the loading rate is very low, resulting in displacement not exceeding 0.1 mm/min. A portable lamp was used to lighten the speckle pattern, and a charge-coupled device (CCD) camera (Basler PiA2400-17gm) was adopted to acquire digital images during the loading process. The camera position was adjusted to make its lens parallel to the specimen surface as much as possible, and the focal length was also adjusted to make the image clear. The resolution of the camera was set to 2448 × 2050 pixels and the length-to-pixel ratio of the imaging system is 0.0588 mm/pixel. The CCD camera was programmed to capture the images automatically at a frame rate of a picture every 50 ms, and this frame rate is suitable to capture and to store a large number of images for further calculations. A typical image recorded is presented on the top right corner of Figure 3.

The crack opening displacement was measured by the COD extensometer device, as seen in Figure 4. Two pieces of metal components were attached onto the rock surface by two sides of the preexisting crack and a sensor was used to gauge the deformation of the perpendicular direction between the metal components. Therefore, the crack opening displacement was obtained during the loading process.

By the DIC method, deformations in Brazilian discs with preexisting cracks under diametral compression test were measured. Three types of specimens with various lengths of the preexisting crack were used in the experimental investigation, which are 15 mm, 20 mm, and 25 mm. The inclination angle (β) of the preexisting crack, as seen in Figure 1(b), was varied to study the effect of the notch orientation on fracture initiation, propagation, the ultimate bearing capacity, and fracture pattern of the discs. The inclination angle varied from 0° to 72° at an interval of 18° per increment.

2.4. Numerical Simulation. Numerical methods are currently the most popular way to simulate the failure process of brittle

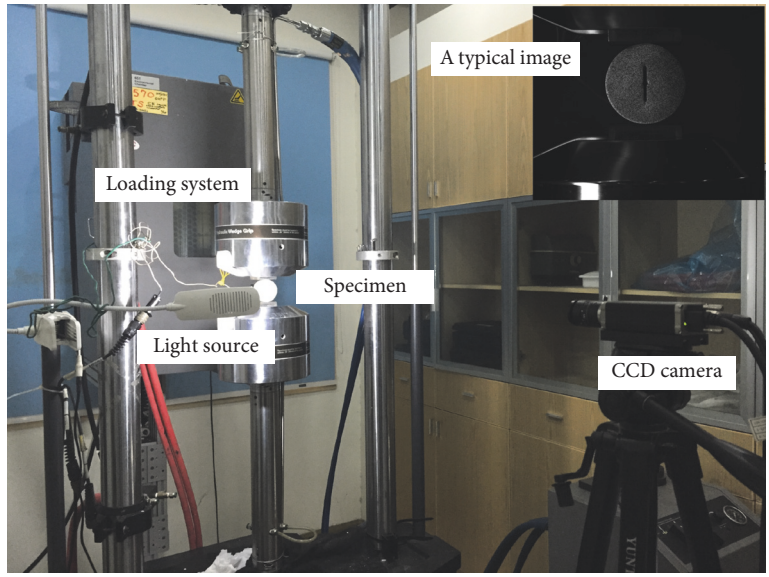

Figure 3: Test equipment of the DIC system.

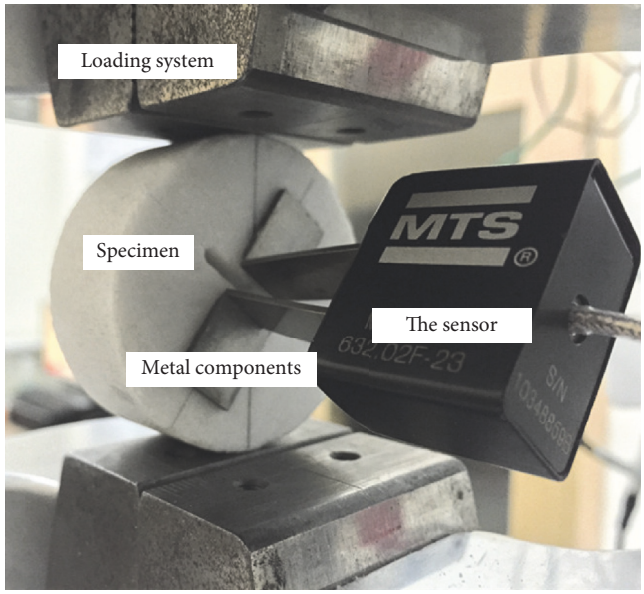

Figure 4: Crack opening displacement extensometer device: metal components and a sensor.

rock. The finite-discrete element combined code ELFEN, developed by Rockfield Software Ltd., was employed in the present study. The ELFEN code simulates the transition of a rock mass from a continuum state to a discontinuous state seamlessly. If the fracture criterion within the intact rock (represented by FEM) is met, a crack (represented by DEM) will be initiated [29]. Recent applications of ELFEN [13, 29] have demonstrated the validity of this FEM-DEM combined approach.

The FEM-DEM combined ELFEN was employed to simulate fracture initiation and propagation in a Brazilian disc with a preexisting crack under diametrical compression. The geometry and size of the numerical model are consistent with those of the specimens in the experiment. Mechanical parameters of marble in Table 1 are also input to compute in the explicit time-integration procedure. The Rankine rotating fracture model, which has two distinct material parameters (tensile strength and fracture energy), is used in our simulation. This model is designed for modelling tensile failure of brittle materials such as rock, glass, and ceramic. For a very brittle material, small fracture energy should be used [13] and we choose 0.1 N/mm for marble in this study. Young's modulus and Poisson's ratio of the loading platens are 200 GPa and 0.2, respectively. The loading platens are modelled as an elastic material, while the discs are modelled as a plastic material. A constant vertical velocity is applied to the upper platen and an equal reverse velocity is also applied to the lower platen to simulate displacement controlled loading. Figure 5 shows the mesh generation in the disc, in which very fine mesh was observed in the vicinity of the preexisting crack where stress concentration is expected.

3. Results and Discussion

3.1. Mechanical Results. Disc specimens with different crack lengths ($2a$ = 15 mm, 20 mm, and 25 mm) were loaded at various inclination angles (β) under static diametral compression, ranging from 0° to 72°. Load, vertical displacement, and crack opening displacement were continually recorded during each test using a computerized data logger. Figure 6 shows the load-vertical displacement relation. As can been seen, if the preexisting crack is parallel to the loading direction (β = 0°), no matter how long the crack is, the load rises again after the first drop and ultimately drops to a really low value. The first drop occurs due to the generation of visible macrocracks and the failure of the notched disc. However, two halves of the broken disc do not fall down

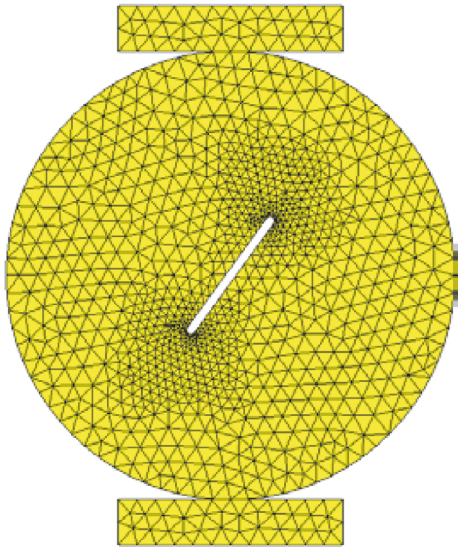

Figure 5: FEM mesh in a Brazilian disc with a preexisting crack in the center.

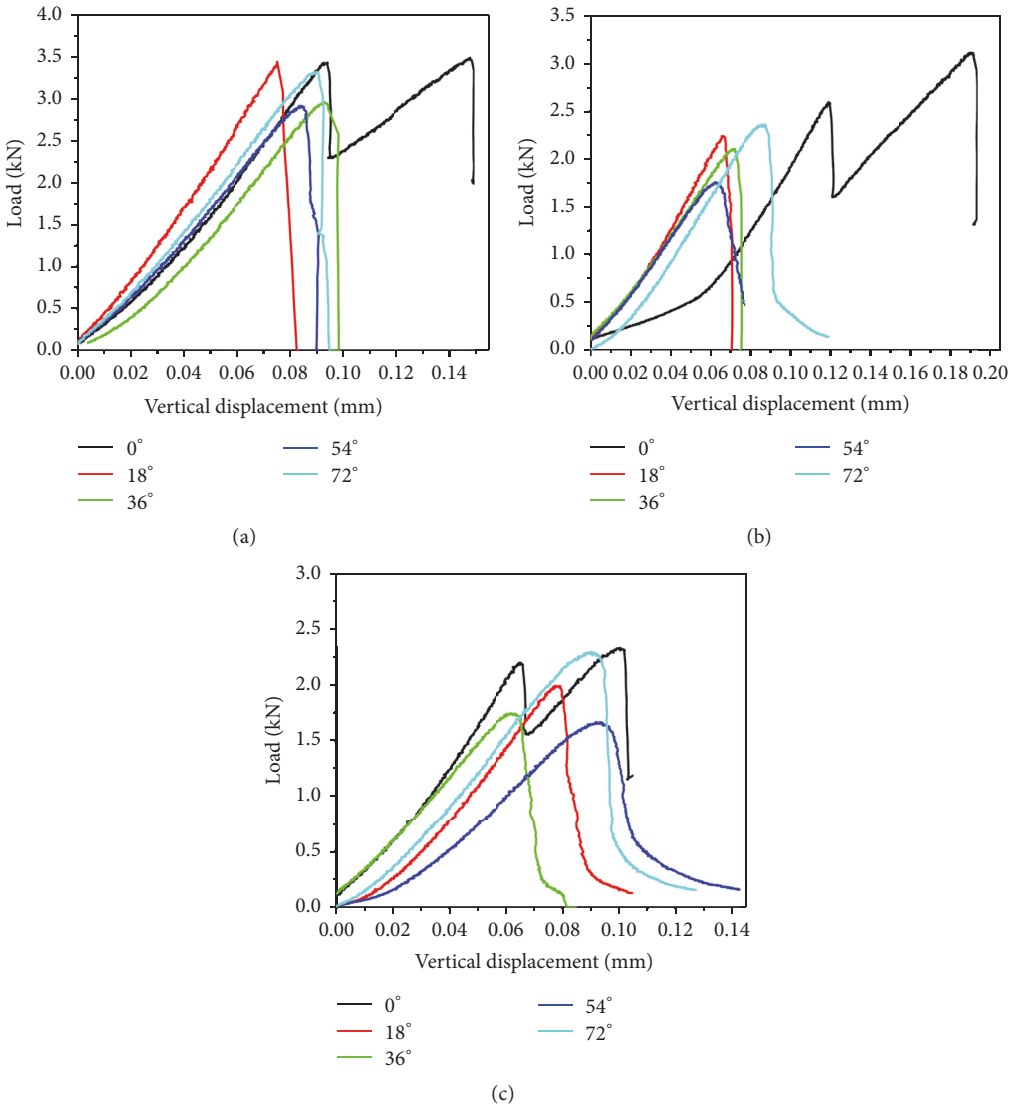

Figure 6: Relationship between load and vertical displacement for each test: (a) $2a = 15$ mm; (b) $2a = 20$ mm; (c) $2a = 25$ mm.

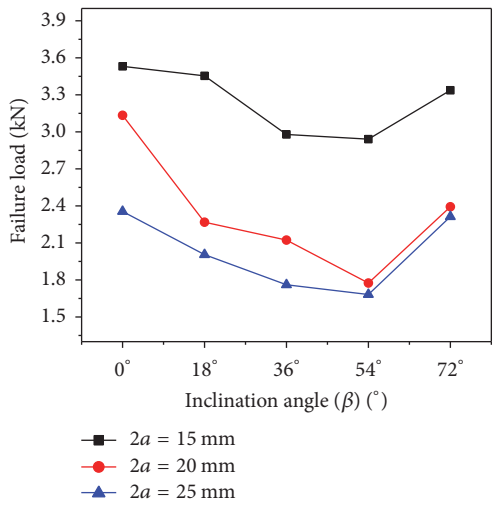

Figure 7: Failure load for the notched discs with preexisting cracks.

because they are clamped by two loading platens. The loading plates are still in contact with the damaged specimen. The applied load continues to rise until the fragments fall down from the loading platform. During this period, a secondary crack is generated. Then, the load declines rapidly again, to a really low value. However, a second rise was not observed in other cases, which perhaps results from the sliding effect during the propagation of the new generated cracks when the preexisting crack is inclined. The fractured disc falls down once the macrocracks run through the specimen and the applied load declines. During the load decline, a secondary crack perhaps occurs. Therefore, only one drop in the load-displacement curve was observed.

Figure 7 gives the ultimate failure load of the notched discs. It is easy to find that the failure load decreases as the crack length increases from 15 mm to 25 mm under a constant inclination angle. This may be due to a shorter rock bridge for longer preexisting crack. Therefore, rock mass with a longer crack is able to carry a lower load. Another interesting finding is that the failure load decreases first and then increases with increasing β and reaches its minimum at the angle of 54°. The reason needs to be further studied theoretically.

3.2. Crack Opening Displacement Results. As shown in Figure 8, the crack opening displacement (COD) was also monitored continuously until failure for each test. It is clear that all the notched cracks opened for values of β up to 18°, no matter how long the crack is. These open cracks result from effective normal tensile stress perpendicular to the crack plane [1]. As seen in Figure 8, for $\beta = 36°$, the notched cracks initially closed slightly and then opened. This slight closing displacement is smaller than 0.005 mm. For $\beta = 54°$, the notched cracks also closed initially and ultimately opened; however, their closing displacement is much greater. The cracks close if they are oriented at an angle of 72°. The cracks with different lengths show a similar response. The opening or closure of the preexisting crack depends more on its orientation than on its length. Another important observation from the COD-time plots is that the crack closing displacement increases with increasing the length of the preexisting crack from 15 mm to 25 mm under a constant inclination angle β (see Figure 9). Under a constant crack length, the closing displacement also increases as the inclination angle increases from 36° to 72°. It is concluded that a more inclined and longer crack facilitates itself to close. As seen in Figure 10, the increment of the maximum closing displacement due to the longer crack Δd_1 is smaller than that owing to the more inclined crack Δd_2. Therefore, it is concluded that the influence of the inclination angle on its closure behavior is greater than that of the length.

The crack opening displacement was also measured by the DIC method. As seen in Figure 11, an "extensometer" was constructed in GOM Correlate to measure the distance between two points (points A and B) located at two sides of the preexisting crack. The direction between these two points is perpendicular to the preexisting crack plane. The result measured by the DIC method is compared with that monitored by the COD extensometer device, and an example is presented in Figure 12. It can be seen that the overall trends of the crack opening displacement measured by the two methods are similar to each other. The crack initially closed and finally opened in this example. It was clearly observed that the COD-time curve by the DIC method is much jittery. In addition, a slight deviation of the exact value of the crack opening displacement between the two methods was also noted. This may be due to the two-dimensional DIC method we used to measure perpendicular distance in plane. There will still be a slight deviation even though the camera position was adjusted to make the camera lens as parallel as possible to the specimen surface. However, the COD extensometer device is a kind of three-dimensional technique to measure the perpendicular direction displacement in three-dimensional space. Therefore, as indicated in Figure 12, the result measured by the DIC method is a little different from that monitored by the COD device. But the variation tendency is coincident. Therefore, the DIC method can also be used to investigate the crack opening displacement of the preexisting crack to some extent.

3.3. Failure Patterns. The deformation evolution process and fracture initiation and propagation were tracked by the DIC system, and five examples with an identical length of the preexisting crack (15 mm) are presented in Table 2. Figure 13 shows the load-vertical displacement relation for the disc specimen with a 15 mm long preexisting crack oriented at 54°, whose principal strain contours during crack propagation are presented in the penultimate line of Table 2, where the load stages correspond to the five marked red points (a, b, c, d, and e) in Figure 13, respectively. Based on the five principal strain contours and the load-displacement curve, five stages were discussed. As seen in Table 2 (a), there is no initial strain around the preexisting crack or somewhere else before the diametrical compression test. It can be seen from the strain contour (b) that high strain zone appears near the two tips of the preexisting crack, which indicates that stress concentration initially occurs around the tips. The tensile

Table 2: Crack propagation and failure patterns for different inclination angles β ($2a$ = 15 mm).

Specimen number	(a)	(b)	(c)	(d)	(e)
M15-1-0°	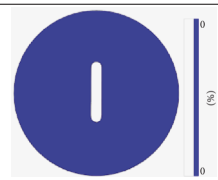	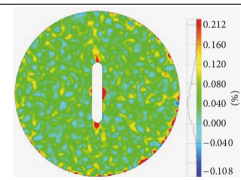	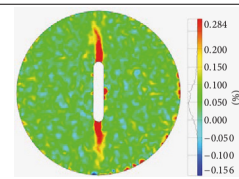	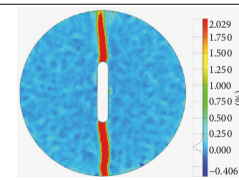	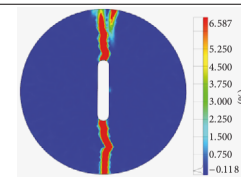
M15-2-18°		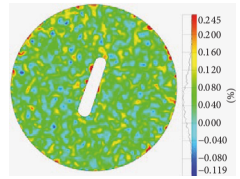	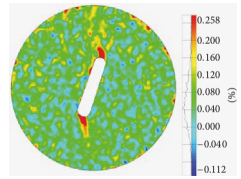	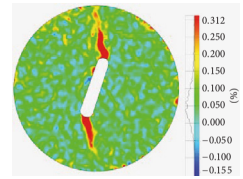	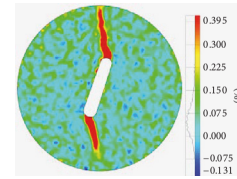
M15-3-36°	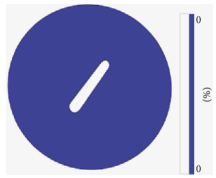	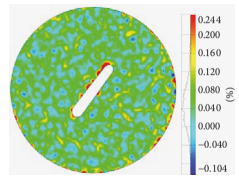	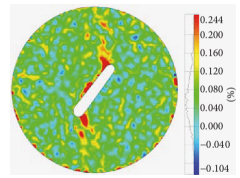	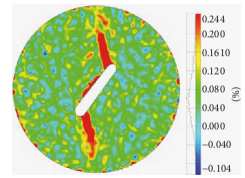	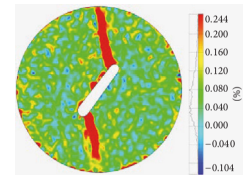
M15-4-54°	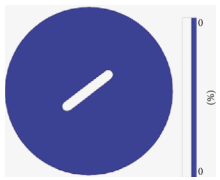	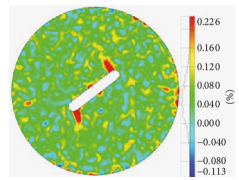	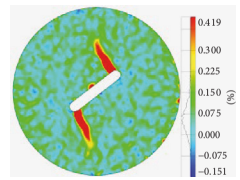	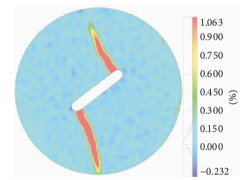	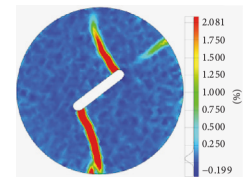
M15-5-72°	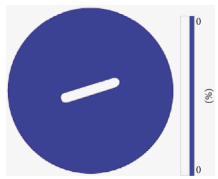	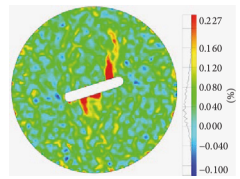	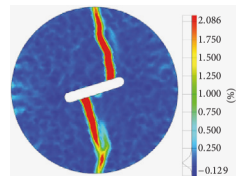	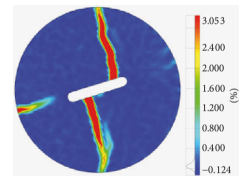	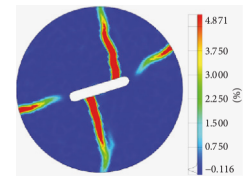

Note. In the specimen number, M means marble, the first number means the length of the preexisting crack, the second number means the serial number, and the third number represents the inclination angle.

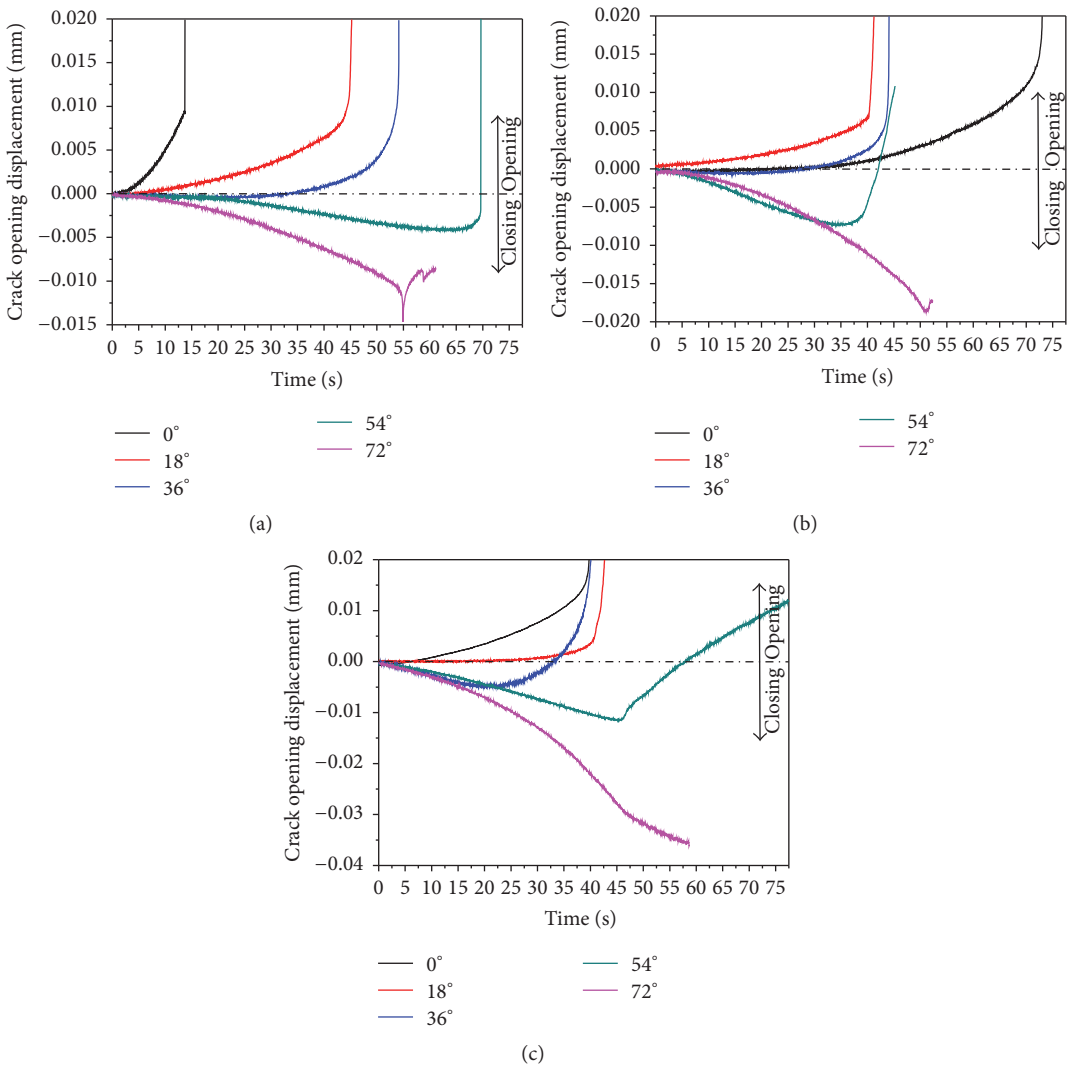

Figure 8: Crack opening displacement for specimens: (a) $2a = 15$ mm; (b) $2a = 20$ mm; (c) $2a = 25$ mm.

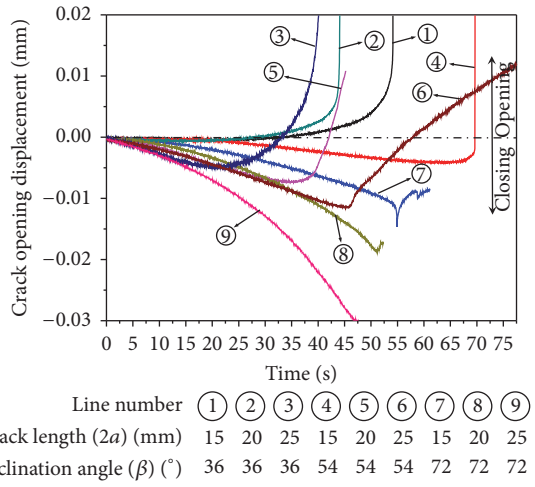

Figure 9: Crack opening displacement for the specimens with preexisting cracks oriented at 36°, 54°, and 72°.

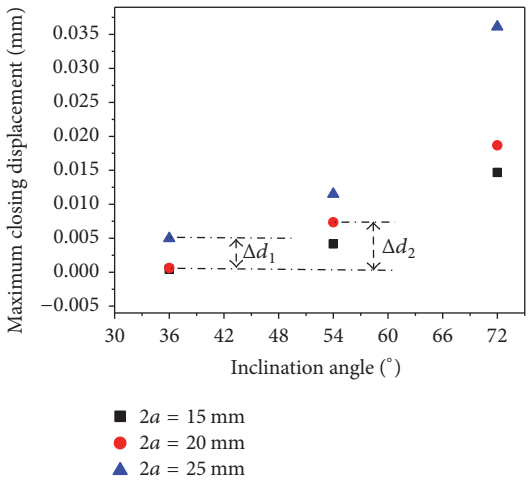

Figure 10: Maximum closing displacement for the specimens with preexisting cracks oriented at 36°, 54°, and 72°.

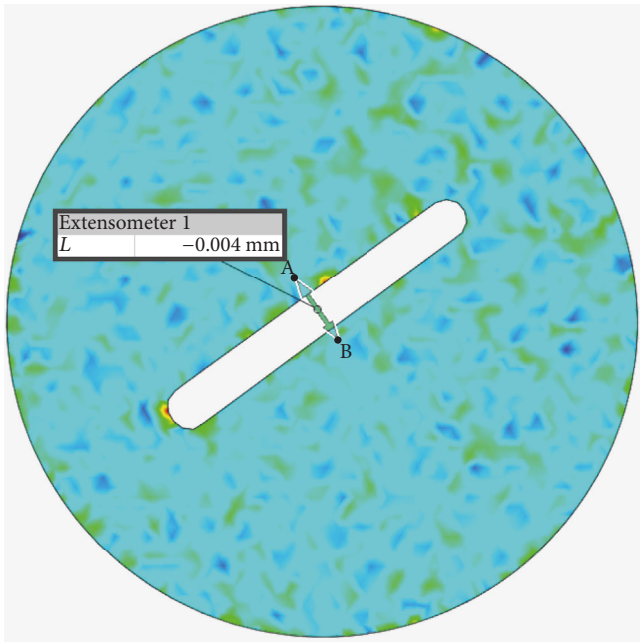

Figure 11: "Extensometer" constructed in GOM Correlate software.

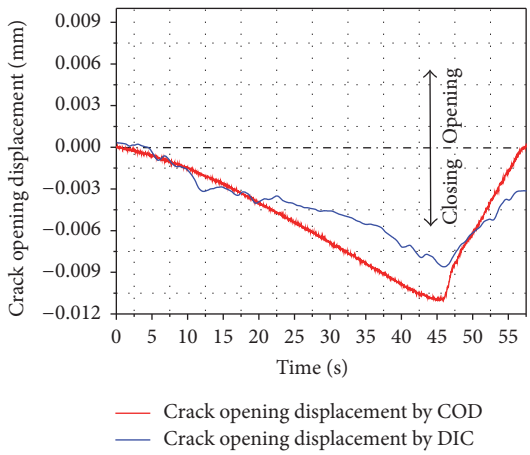

Figure 12: Crack opening displacement for the disc with a 25 mm long preexisting crack oriented at 54° measured by COD device and DIC method.

strength of marble is 4.97 MPa; therefore, the limit strain is calculated by (1) according to the second strength theory:

$$\varepsilon_{\text{lim}} = \frac{\sigma}{E}, \quad (1)$$

where ε_{lim} is limit strain, σ is tensile strength, and E is elastic modulus. The limit strain is $120 * 10^{-6}$, while the maximum strain in (b) is $2260 * 10^{-6}$ from the legend in the right corner, which exceeds the limit strain evidently. Therefore, several microcracks initiate near the tips of the preexisting crack. The minimum principle stress distribution based on numerical simulation at the two loading stages is presented in Figure 14 (positive as tension). At the moment corresponding

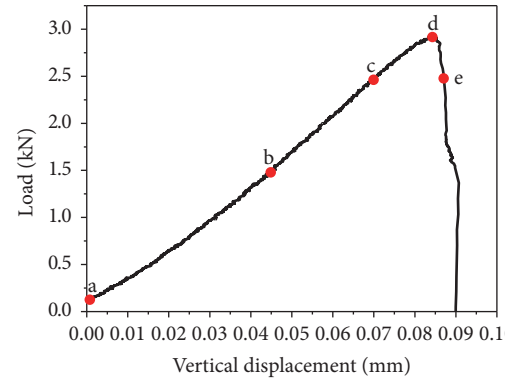

Figure 13: Relationship between load and vertical displacement for $\beta = 54^{\circ}$ and $2a = 15$ mm.

to column (b) in Table 2, the stress distribution is shown in Figure 14(a). It can be seen that high tensile stress zones occur near the tips of the preexisting crack. When tensile stress reaches tensile strength of the material, wing cracks are initiated. Wing cracks were clearly observed in column (c), Table 2. The propagation track of the new generated cracks progressively gets close to the maximum compressive stress direction. As seen in (d), the wing cracks penetrate the whole specimen. At this time, the load reaches its peak value and then it decreases quickly. Meanwhile, the macroscopic fracture was observed. High tensile stress zones move to the disc boundary thereafter (in Figure 14(b)). Then, a secondary crack, which is subparallel to the preexisting plane, starts to appear from the disc boundary and propagates towards the tips of the preexisting crack, as seen in (e), at a load level of about 4/5 of the peak load in Figure 13. Therefore, wing cracks and secondary cracks are both tensile in nature, which is supported by a previous study [13]. The white (empty) areas indicate compression zones due to the specific contour ranges of 0–5 MPa. It is clearly seen that the compression zones occur at the loading end and in the opposite locations of tensile stress concentration, which is supported by a previous study [30].

3.4. Discussions. The influence of the inclination angle β on crack initiation, propagation, and final failure patterns is summarized in Table 2. It can be seen that high strain zones initially occur around the tips of the preexisting crack and the high strain zones eventually break through the notched disc. If the preexisting crack is parallel to the loading direction, the new cracks initiate at the tips and propagate along the loading direction. Secondary cracks were also observed at the loading end. For the cracks with small inclination angle ($\beta = 18^{\circ}$), the wing cracks also initiate at the tips. As the inclination angle β increases, the wing cracks initiation positions deviate from the tips and move towards the disc center. It is a pity that the occasion in which $\beta = 90^{\circ}$ was not included in our experiment. Therefore, a numerical simulation was performed and the final result is shown in Figure 15. It can be seen that there is a limit to bound the wing crack initiation position even if the preexisting crack is perpendicular to

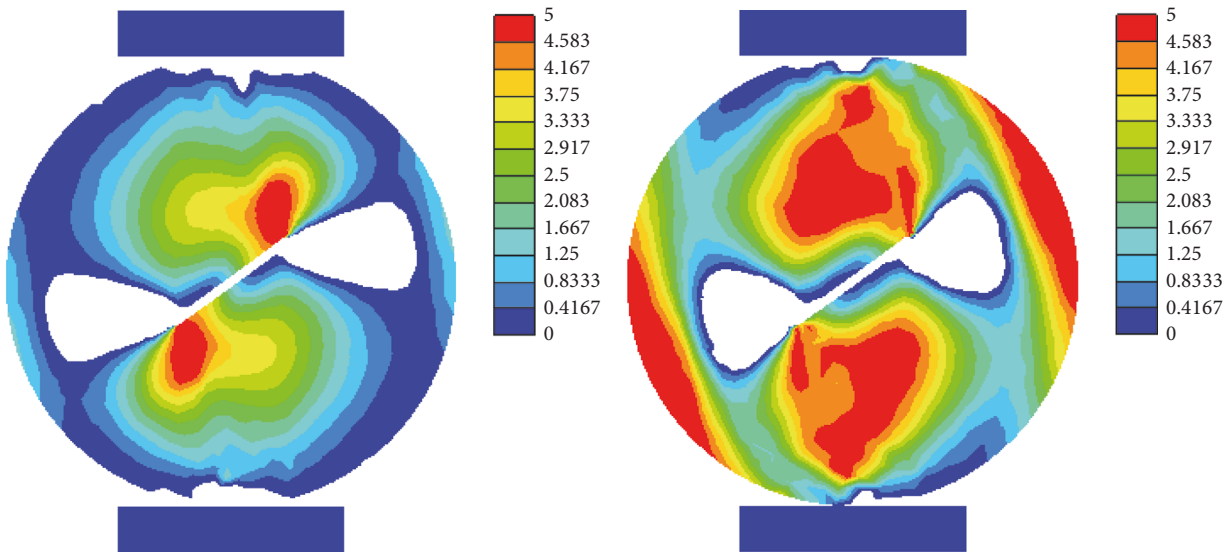

Figure 14: Distribution of the minimum principal stress (unit: MPa) for $\beta = 54^{\circ}$ and $2a = 15$ mm: (a) stage before wing cracks are inserted; (b) stage before secondary cracks are inserted.

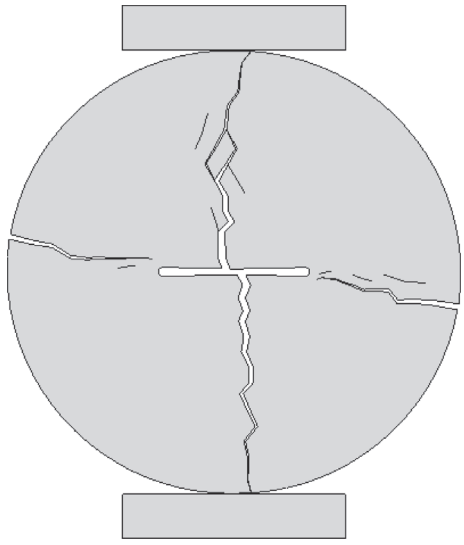

Figure 15: Failure pattern for the specimen with a preexisting crack oriented at 90° ($2a = 15$ mm) based on numerical simulation.

the loading direction. The wing cracks will not start from the disc center due to the existence of the defect. As load increases, the wing cracks propagate towards the loading platens. The secondary cracks, which are subparallel to the preexisting crack, were observed only when the inclination angle is relatively large, that is, 54° and 72°, after the wing cracks run through the specimen. A secondary crack also occurs if the inclination angle is 0°; however, this is because the broken specimen is clamped by the loading platens.

The final failure pictures, the ultimate principal strain contours, and the results from numerical simulation are summarized in Table 3. It is clearly seen that three subfigures match each other well, and the effectiveness and validity of the digital image analysis can be proved. However, no visible macrocrack was observed in the final failure pictures for three specimens: M20-4-54, M20-5-72, and M25-5-72. Actually, damage does exist and it can be clearly seen by the utilization of the DIC method. No visible macrocrack on the pictures may be due to the restraint from the paint sprayed onto the rock surface. This further confirms the superiority of the DIC method. Table 3 shows the ultimate failure patterns for discs with various lengths ($2a = 15$ mm, 20 mm, and 25 mm) oriented at 36°, 54°, and 72°. For the cracks inclined at 36°, a secondary crack only occurs if the length of the preexisting crack is 25 mm, and only a single one appears on one side from the disc boundary. For the cracks oriented at 54°, secondary cracks occur in discs with all length cracks. An individual secondary crack appears in the disc with a 15 mm long preexisting crack, while a pair of secondary cracks occur in the specimens with longer preexisting cracks, that is, 20 mm and 25 mm. If the inclination angle β is 72°, pairs of secondary cracks appear no matter how long the preexisting crack is. Therefore, it is concluded that a more inclined and longer preexisting crack facilitates the generation of secondary cracks. In addition, that the length of the preexisting crack takes no effect on the new generated cracks initiation and propagation was also inferred.

4. Conclusion

The fracture process of Brazilian discs with different lengths preexisting cracks oriented at various angles, that is, 0°, 18°, 36°, 54°, and 72°, was investigated with the aid of the DIC method in the present study. The DIC method reveals the initiation and propagation of the primary wing cracks

Table 3: Comparison of DIC analysis, failure pictures, and simulation results.

Specimen number	DIC analysis	Failure pictures	Simulation results
M15-3-36	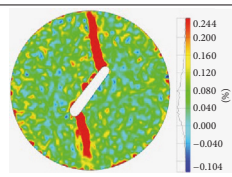		
M20-3-36	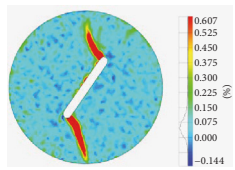		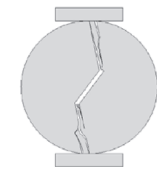
M25-3-36	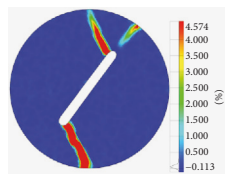	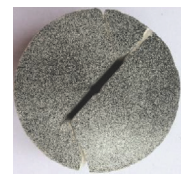	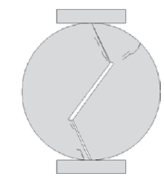
M15-4-54	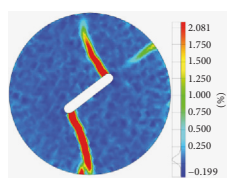		
M20-4-54	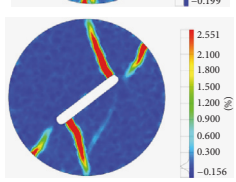		
M25-4-54	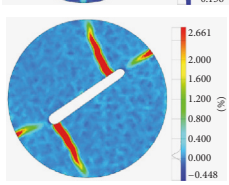		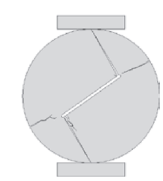
M15-5-72	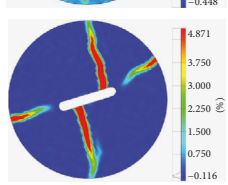		
M20-5-72	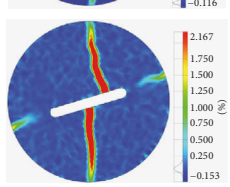		
M25-5-72	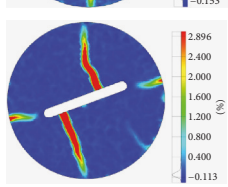		

Note. In the specimen number, M means marble, the first number means the length of the preexisting crack, the second number means the serial number, and the third number represents the inclination angle.

and secondary cracks explicitly. The results show that the bearing capacity and failure patterns of the notched discs are greatly affected by the inclination angle and the length of the preexisting crack.

The bearing capacity of the notched discs exhibits an early decrease and later increasing trend with increasing inclination angle and the peak load obviously decreases for a longer preexisting crack. Both of the opening or closure of the preexisting crack and its maximum closing displacement are influenced by the inclination angle and the length. Moreover, the effect of the orientation is much greater. The initiation position of the primary wing crack deviates from the tips of the preexisting crack as the inclination angle increases; however, the length seems to make no difference. A more inclined and longer preexisting crack facilitates the generation of secondary cracks.

Although the numerical simulation method is currently more and more popular, field tests and laboratory experiments will not be replaced by numerical simulation methods. A full-field strain distribution and its evolution process can be presented by the DIC method, in which the observation of crack initiation and propagation can be easily realized during in situ tests and laboratory experiments. In addition, the DIC method can also be used to monitor the crack opening displacement. In general, this method will be a good choice for the investigation on the damage evolution mechanism of the fractured rock and it also provides a good way to establish the constitutive model for the jointed rock.

Conflicts of Interest

The authors declare that they have no conflicts of interest regarding the publication of this paper.

Acknowledgments

The authors acknowledge the financial supports of the National Natural Science Foundation of China (11472311 and 41630642) and the Fundamental Research Funds for the Central Universities of Central South University (2017zzts166).

References

[1] N. Erarslan and D. J. Williams, "Mixed-mode fracturing of rocks under static and cyclic loading," *Rock Mechanics and Rock Engineering*, vol. 46, no. 5, pp. 1035–1052, 2013.

[2] J. Zhou, X. Z. Shi, and X. B. Li, "Utilizing gradient boosted machine for the prediction of damage to residential structures owing to blasting vibrations of open pit mining," *Journal of Vibration and Control*, vol. 22, no. 19, pp. 3986–3997, 2016.

[3] J. Zhou, X. Li, and H. S. Mitri, "Classification of rockburst in underground projects: Comparison of ten supervised learning methods," *Journal of Computing in Civil Engineering*, vol. 30, no. 5, Article ID 04016003, 2016.

[4] E. Hoek, P. Kaiser, and W. Bawden, *Support of Underground Excavations in Hard Rock*, Balkema, Rotterdam, Netherlands, 1995.

[5] ISRM, "Suggested methods for determining tensile strength of rock materials," *International Journal of Rock Mechanics and Mining Sciences & Geomechanics Abstracts*, vol. 15, no. 3, pp. 99–103, 1978.

[6] Z. Zhou, X. Li, Y. Zou, Y. Jiang, and G. Li, "Dynamic Brazilian tests of granite under coupled static and dynamic loads," *Rock Mechanics and Rock Engineering*, vol. 47, no. 2, pp. 495–505, 2014.

[7] J. Qiu, D. Li, and X. Li, "Dynamic failure of a phyllite with a low degree of metamorphism under impact Brazilian test," *International Journal of Rock Mechanics and Mining Sciences*, vol. 94, pp. 10–17, 2017.

[8] L. Luo, X. Li, M. Tao, and L. Dong, "Mechanical behavior of rock-shotcrete interface under static and dynamic tensile loads," *Tunnelling and Underground Space Technology*, vol. 65, pp. 215–224, 2017.

[9] H. Awaji and S. Sato, "Combined mode fracture toughness measurement by the disk test," *Journal of Engineering Materials and Technology*, vol. 100, no. 2, pp. 175–182, 1978.

[10] C. Atkinson, E. Smelser R, and J. Sanchez, "Combined mode fracture via the cracked brazilian disk test," *International Journal of Fracture*, vol. 18, no. 4, pp. 279–291, 1982.

[11] Z. Jia, A. Castro-Montero, and S. P. Shah, "Observation of mixed mode fracture with center notched disk specimens," *Cement and Concrete Research*, vol. 26, no. 1, pp. 125–137, 1996.

[12] M. R. M. Aliha, M. R. Ayatollah, D. J. Smith, and M. J. Pavier, "Geometry and size effects on fracture trajectory in a limestone rock under mixed mode loading," *Engineering Fracture Mechanics*, vol. 77, no. 11, pp. 2200–2212, 2010.

[13] M. Cai, "Fracture initiation and propagation in a brazilian disc with a plane interface: a numerical study," *Rock Mechanics and Rock Engineering*, vol. 46, no. 2, pp. 289–302, 2013.

[14] J. S. Epstein and M. S. Dadkhah, "Moire interferometry in fracture research," *Experimental Techniques in Fracture*, pp. 427–508, 1993.

[15] R. J. Sanford, "Determining fracture parameters with full-field optical methods," *Experimental Mechanics*, vol. 29, no. 3, pp. 241–247, 1989.

[16] E. A. Patterson and E. J. Olden, "Optical analysis of crack tip stress fields: a comparative study," *Fatigue and Fracture of Engineering Materials and Structures*, vol. 27, no. 7, pp. 623–636, 2004.

[17] S. P. Ma, X. H. Xu, and Y. H. Zhao, "The GEO-DSCM system and its application to the deformation measurement of rock materials," *International Journal of Rock Mechanics and Mining Sciences*, vol. 41, pp. 292–297, 2004.

[18] C. Zhao, H. Matsuda, C. Morita, and M. R. Shen, "Study on failure characteristic of rock-like materials with an open-hole under uniaxial compression," *Strain*, vol. 47, no. 5, pp. 405–413, 2011.

[19] H. Munoz, A. Taheri, and E. K. Chanda, "Pre-Peak and post-peak rock strain characteristics during uniaxial compression by 3d digital image correlation," *Rock Mechanics and Rock Engineering*, vol. 49, no. 7, pp. 2541–2554, 2016.

[20] Q. Lin, L. Biolzi, and J. F. Labuz, "Opening and mixed-mode fracture initiation in a quasi-brittle material," *Journal of Engineering Mechanics*, vol. 139, no. 2, pp. 177–187, 2012.

[21] Q. Lin, H. Yuan, L. Biolzi, and J. F. Labuz, "Opening and mixed mode fracture processes in a quasi-brittle material via digital imaging," *Engineering Fracture Mechanics*, vol. 131, pp. 176–193, 2014.

[22] W. W. Ji, P. Z. Pan, Q. Lin et al., "Do disk-type specimens generate a mode II fracture without confinement?" *International*

Journal of Rock Mechanics and Mining Sciences, vol. 87, pp. 48–54, 2016.

[23] W. Ji, Pan Z. P., and Miao T. X., "Fracture characteristics of two fypes of rocks based on digital image correlation," in *Rock and Soil Mehcanics*, vol. 37, pp. 2299–2305, Rock and Soil Mehcanics, 2016.

[24] Sutton M. A., J. j. Orteu, and H. Schreier, *MediaImage correlation for shape, motion and deformation measurements: basic concepts, theory and applications*, Springer Science & Business, 2009.

[25] H. Song, H. Zhang, Y. Kang, G. Huang, D. Fu, and C. Qu, "Damage evolution study of sandstone by cyclic uniaxial test and digital image correlation," *Tectonophysics*, vol. 608, pp. 1343–1348, 2013.

[26] G. Yang, Z. Cai, X. Zhang, and D. Fu, "An experimental investigation on the damage of granite under uniaxial tension by using a digital image correlation method," *Optics and Lasers in Engineering*, vol. 73, pp. 46–52, 2015.

[27] B. Pan, K. Qian, H. Xie, and A. Asundi, "Two-dimensional digital image correlation for in-plane displacement and strain measurement: a review," *Measurement Science and Technology*, vol. 20, no. 6, Article ID 062001, 2009.

[28] Q. Lin and J. F. Labuz, "Fracture of sandstone characterized by digital image correlation," *International Journal of Rock Mechanics and Mining Sciences*, vol. 60, pp. 235–245, 2013.

[29] M. Cai and P. K. Kaiser, "Numerical simulation of the Brazilian test and the tensile strength of anisotropic rocks and rocks with pre-existing cracks," *International Journal of Rock Mechanics and Mining Sciences*, vol. 41, pp. 478–483, 2004.

[30] H. Y. Liu, S. Q. Kou, P. A. Lindqvist, and C. A. Tang, "Numerical modelling of the heterogeneous rock fracture process using various test techniques," *Rock Mechanics and Rock Engineering*, vol. 40, no. 2, pp. 107–144, 2007.